crystals

MDPI

Article

Ultrahigh Electromechanical Coupling and Its Thermal Stability in $(Na_{1/2}Bi_{1/2})TiO_3$-Based Lead-Free Single Crystals

Chao Chen [1,2,*], Li Yang [1], Xingan Jiang [1], Xiaokun Huang [1], Xiaoyi Gao [2], Na Tu [1], Kaizheng Shu [1], Xiangping Jiang [1], Shujun Zhang [2] and Haosu Luo [3]

1 Jiangxi Key Laboratory of Advanced Ceramic Materials, National Engineering Research Center for Domestic & Building Ceramics, School of Materials Science and Engineering, Jingdezhen Ceramic Institute, Jingdezhen, Jiangxi 333403, China; yangli5799@163.com (L.Y.); jiangxa88@163.com (X.J.); 031203@jci.edu.cn (X.H.); tuna_618@163.com (N.T.); shukaizheng@jci.edu.cn (K.S.); 001037@jci.edu.cn (X.J.)

2 Institute for Superconducting and Electronic Materials, Australian Institute for Innovative Materials, University of Wollongong, North Wollongong 2500, Australia; xygao@whut.edu.cn (X.G.); shujun@uow.edu.au (S.Z.)

3 Artificial Crystal Research Center, Shanghai Institute of Ceramics, University of Chinese Academy of Sciences, Jiading, Shanghai 200050, China; hsluo@mail.sic.ac.cn

* Correspondence: 001627@jci.edu.cn

Received: 7 May 2020; Accepted: 27 May 2020; Published: 29 May 2020

Abstract: In this work, we report the ultrahigh electromechanical coupling performance of NBT-6BT-KNN lead-free single crystal at room temperature. The thickness mode electromechanical coupling coefficient (k_t) and the 31 mode electromechanical coupling coefficient (k_{31}) reach 69.0% and 45.7%, respectively, which are superior to the PZT-5H lead-based ceramics of k_t~60% and k_{31}~39%. In addition, the evolution of the crystal structure and domain morphology is revealed by Raman scattering spectra, a polarizing microscope and piezoelectric force microscopy characterization.

Keywords: lead-free single crystal; NBT-based; electromechanical coupling; phase transition; domain structure

1. Introduction

Piezoelectric materials, which convert mechanical to electrical energy (and vice versa), are crucial in sensors, actuators, transducers, and ultrasonic devices [1–3]. Lead zirconium titanate (PZT) based ceramics are currently market-dominating due to their excellent piezoelectric properties [4,5]. However, these PZT family materials contain toxic lead, which is restricted in view of the environment. Great efforts have been made worldwide to seek alternative lead-free piezoelectric materials [6–8]. The essential strategy for achieving a high piezoelectric response is to seek lead-free materials displaying a transition region in their composition phase diagrams, known as a morphotropic phase boundary (MPB), where energetically comparable polar states coexist and compete with each other [6,7]. Such critical energy landscapes cause a fragility and instability of the polar state, so that the polarization can be easily rotated and altered by external stress or electric field. Some developments in the search for lead-free piezoelectric materials are $BaTiO_3$-based, $(K_{1/2}Na_{1/2})NbO_3$-based, and $Na_{1/2}Bi_{1/2}TiO_3$-based systems approached by constructing an MPB [6,9,10]. It was later discovered that an MPB could be also created through external mechanical stress or electrical field, which results in a strong piezoelectric response [11,12]. Electric-field in situ Transmission Electron Microscopy (TEM) has revealed that the overall poling-induced phase transitions in $0.94Na_{1/2}Bi_{1/2}TiO_3$-$0.06BaTiO_3$ ceramics can be described as R3c/P4bm→P4mm/R3c→R3c [11]. Ge et al. and Daniels et al. proposed

that an E-field induced phase transformation from pseudo cubic to T structure is responsible for the large electrically induced strain [13,14]. Recently, Wang et al. [15] reported a ternary lead-free $Na_{1/2}Bi_{1/2}TiO_3$-$BaTiO_3$-$(K_{1/2}Na_{1/2})NbO_3$ (NBT-BT-KNN) single crystal that exhibits an unprecedented piezoelectric coefficient of $d_3 \approx 840$ pC N^{-1}. The origin of the high piezoelectricity is attributed to a phase boundary constructed by the poling field between multiple weak-polar *R*3c/*P*4bm phases and ferroelectric tetragonal phases with *P*4mm symmetry.

The electromechanical coupling coefficient is an important parameter which characterizes the coupling between the mechanical energy and electrical energy of piezoelectric materials. However, the electromechanical coupling coefficient of this ternary NBT-BT-KNN single crystal has not yet been presented. In this communication, we report the ultrahigh electromechanical coupling performance of NBT-6BT-KNN single crystal. The thickness mode electromechanical coupling coefficient (k_t) and the 31-mode electromechanical coupling coefficient (k_{31}) reach 69.0% and 45.7%, respectively, which are superior to the PZT-5H lead-based ceramics of $k_t \sim 60\%$ and k_{31}~39%. The temperature-dependent k_t and k_{31} are further studied, which reveals a mechanism for temperature-induced phase transition.

2. Materials and Methods

$(0.94-x)(Na_{1/2}Bi_{1/2})TiO_3$-$0.06BaTiO_3$-$xK_{1/2}Na_{1/2}NbO_3$ (NBT-6BT-100xKNN, x = 0.01) single crystals were grown by a carefully controlled TSSG technique. The raw materials of K_2CO_3 (99.99%), Na_2CO_3 (99.99%), Bi_2O_3 (99.999%), $BaCO_3$ (99.99%), Nb_2O_5 (99.99%), and TiO_2 (99.99%) were weighed according to the nominal ratio of NBT-6BT-KNN. Then the well-mixed compounds were put into a platinum (Pt) crucible and calcined at 850 °C for 3 h in air to form the NBT-6BT-KNN polycrystalline precursor. Then, the polycrystalline materials were ground and mixed with excess ~20 wt% Na_2CO_3, K_2CO_3, and Bi_2O_3 as a self-flux. Single crystals were grown using a <001> direction seed in a Pt crucible, which was heated to ~1300 °C using a resistance furnace under an air atmosphere. The details of crystal growth can be found elsewhere [15]. The x-ray fluorescence analyzer (XRFA) and x-ray diffraction (XRD) were utilized to determine the real composition and phase structure of the as-grown crystal, respectively.

For the macroscopic electrical characterization, the as-grown single crystals were sliced into wafers with a thickness of ~0.40 mm, perpendicular to their pseudo cubic <100> directions. Based on the IEEE standards, the [001]-oriented crystal planes with a size of $4 \times 4 \times 0.4$ mm^3 were cut to obtain thickness mode samples. The 31 mode samples were cut into rectangular parallelepiped shapes along with crystallographic directions of [100]/[010]/[001] with a size of $12.3 \times 2.4 \times 0.4$ mm^3. Then, the main faces of the samples were sputtered with gold electrodes. The crystal samples were poled in silicon oil at room temperature for 15 min with a dc electric field of 25 kV cm^{-1}. Dielectric/loss-temperature and impedance-phase angle measurements were conducted using a computer-controlled Novel control cmbH Concept 40 broadband dielectric spectrometer. Raman measurements were conducted at room temperature using a Raman spectrometer (LabRAM HR800, Horiba JobinYvon, Paris, France). The domain structure was observed using an Olympus (Tokyo, Japan) U-CMAD3 polarizing microscope (PLM) equipped with a Linkam THMS600E (Linkam Scientific Instruments Ltd.,Tadworth, Surrey, U.K). The PLM is used in transmission geometry, and the principle of setup in our case was as follows: we defined the "θ" as the angle between the polarizer/analyzer (P/A) pair and the pseudo cubic <100> direction. For the domains of the tetragonal phase, the optical extinction is achieved when the P/A is set along the <100> direction, namely at θ = 0° with respect to the <100> direction. For the domains of the rhombohedral phase, they exhibit optical extinction when the P/A is set along the <110> direction, namely at θ = 45° with respect to the <100> direction. The PFM experiments were carried out using a commercial atomic force microscope MFP-3D (Asylum Research, Goleta, USA). An ac modulation voltage of 7 V (peak to peak) with a frequency of 10 kHz was applied between the conductive tip and the bottom gold electrode.

3. Results and Discussion

Figure 1a,b shows the thickness mode and 31 mode impedance and phase angle of the poled NBT-6BT-KNN crystal along the <001> direction at room temperature, respectively. It is clear from the figure that the phase angle of NBT-6BT-KNN crystal in the two modes is close to 80°, indicating the completely polarized state. The electromechanical coupling coefficients k_t and k_{31} are calculated by the resonance-antiresonance method (as shown in Formula (1), (2)), which are 69.0% and 45.7%, respectively, superior to those of k_t ~ 60% and k_{31}-39% of PZT-5H lead-based ceramics [16]. We have also compared our own results in this work to the results from full sets of electromechanical constants of other lead-free ferroelectric (piezoelectric) ceramic/single crystals; details can be seen in Table 1 [16–21].

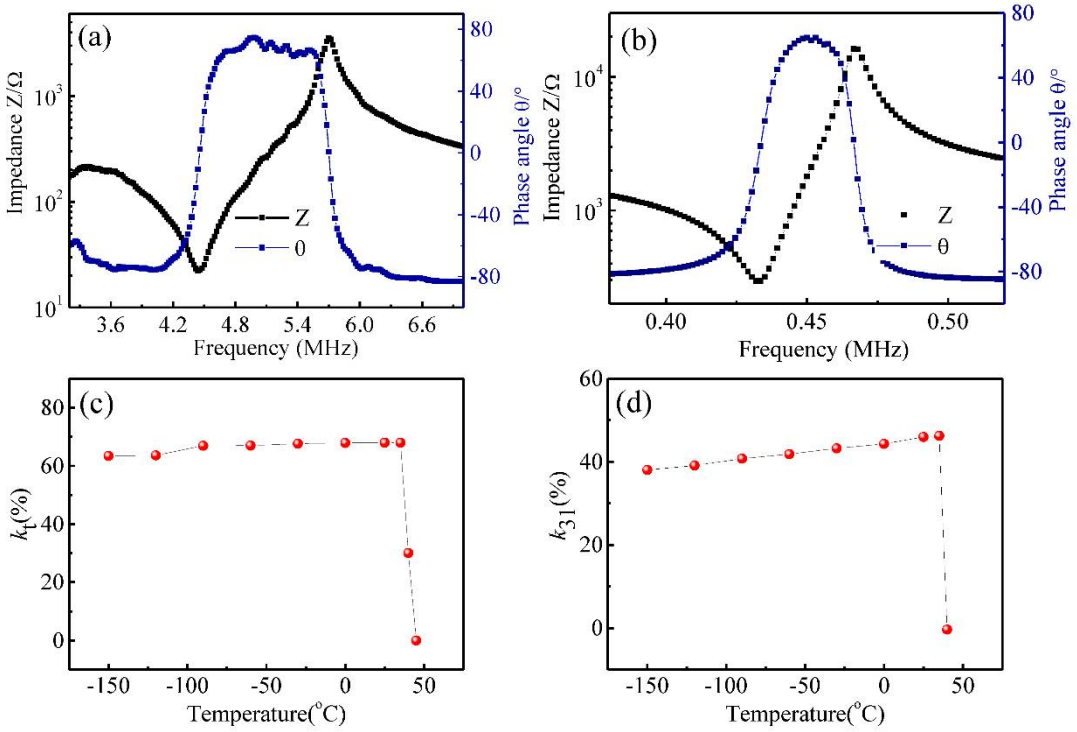

Figure 1. (**a**) the thickness mode and (**b**) 31 mode impedance and phase angle of the poled NBT-6BT-KNN crystal along the <001> direction at room temperature; the temperature dependent behavior of (**c**) k_t and (**d**) k_{31}.

Table 1. Comparison of the properties of previously reported ceramic/single crystals.

Matrials	k_{31}	kt	Quasi-Static d_{33} (pC/N)	Reference
Ceramics				
PZT-5H	39%	60%	-	[16]
KNN-TL	16%	34%	174	[17]
Single crystal				
KNN-T	46%	64.60%	162	[18]
KNN-TL	47%	45.10%	354	[18]
KNN-TL:Mn	59%	49%	630	[19]
NBT-0.053BT/epoxy 1-3 composite	-	73%	360	[20]
NBT-5BT	34.10%	54%	360	[21]
NBT-6BT-KNN	45.70%	69%	840	This work

$$k_t = \sqrt{\frac{\pi}{2}\frac{f_r}{f_a}\tan\left(\frac{\pi}{2}\frac{f_a - f_r}{f_a}\right)} \quad (1)$$

$$k_{31} = \sqrt{\frac{1}{1 - \frac{\tan[(\pi/2)(f_a/f_r)]}{(\pi/2)(f_a/f_r)}}} \quad (2)$$

Figure 1c,d shows the temperature-dependent behavior of k_t and k_{31}, respectively. It is clear from the figures that k_t and k_{31} exhibit good temperature stability within this temperature range between −150 and 40 °C, indicating an excellent cryogenic electromechanical coupling property and a promising candidate for advanced electromechanical transducer applications below room temperature. When the temperature reaches above 45 °C, the value of k_t and k_{31} degenerates sharply to zero. We also measured the temperature-dependent dielectric constant and dielectric loss curves of <001> poled oriented NBT-6BT-KNN crystal at different frequencies, as shown in Figure 2. In general, two dielectric anomalies can be observed during the heating process. The temperature corresponding to the maximum dielectric constant is considered to be the phase transition temperature from the tetragonal phase to the tetragonal + cubic two phase region [10], and the dielectric anomaly at low temperature around 150 °C range shows strong relaxation characteristics of dielectric broadening and frequency dispersion, which are closely related to the polar nanoscale (PNRs) transition from the R3c to the tetragonal P4bm phase according to the TEM results of NBT-based ceramics. These PNRs in the R3c or P4bm phase have a strong relaxation and show a weak/non-polar state [22]. It should be noted that a discontinuous variation in dielectric/loss curves can be only observed in poled crystal and the anomaly also appears exactly at 45 °C, defined as depolarization temperature (T_d). This is well consistent with the degeneration temperature of k_t and k_{31}. The reason for this observation is most likely that the electric field induces the transformation from the weak/non-polar pseudocubic phases (*R*3c/*P*4bm) to the polar tetragonal phase (*P*4mm) and heating causes the tetragonal polar phase to transform back to the non-polar phases [15].

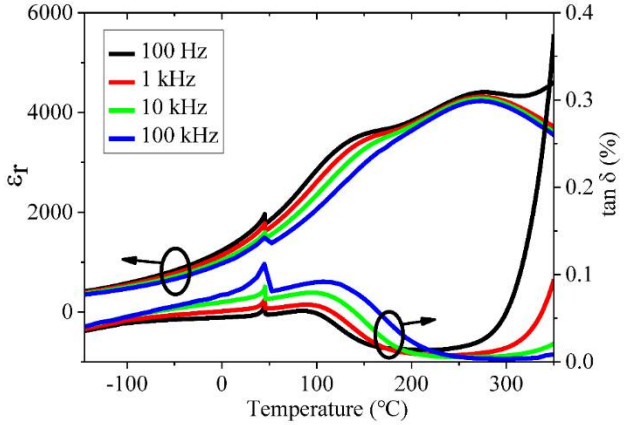

Figure 2. The temperature dependent dielectric constant and dielectric loss curves of poled <001> oriented NBT-6BT-KNN crystal measured at different frequencies.

In order to verify this assumption, we observe the domain evolution of <001> oriented NBT-6BT-KNN crystals under different electric fields and temperatures using a polarizing microscope, as shown in Figure 3. At zero electric field (E = 0 kV/cm), NBT-6BT-KNN crystals show complete light extinction, indicating the initial pseudocubic non-polar state. This is consistent with the XRD result of as-grown NBT-6BT-KNN crystal powder (Figure 4). The diffraction pattern shows no profile shape asymmetry or splitting at any reflections, revealing that the sample is an initial cubic or pseudo cubic structure. When the electric field increases to 25 kV/cm, obvious macroscopic ferroelectric

domains are present for P/A: 45° (θ = 45°), indicating that the electric field induces the phase transition from a non-polar pseudocubic phase to a ferroelectric polar phase [15,23]. The red dotted line and arrows in Figure 3b show the single domain area and crystal cracks, respectively. When the electric field is removed, the ferroelectric domains are still maintained (Figure 3c), revealing that the polar phase is stable after removing the electric field. In addition, as shown in the inset of Figure 3c, the optical extinction of these domains for P/A: 0° (θ = 0°) indicates that the polar phase belongs to the *P*4mm symmetry. When the temperature is increased above T_d (T = 50 °C), the ferroelectric domain disappears completely, as presented in Figure 3d, which confirms the temperature induced a transition back to the non-polar phases.

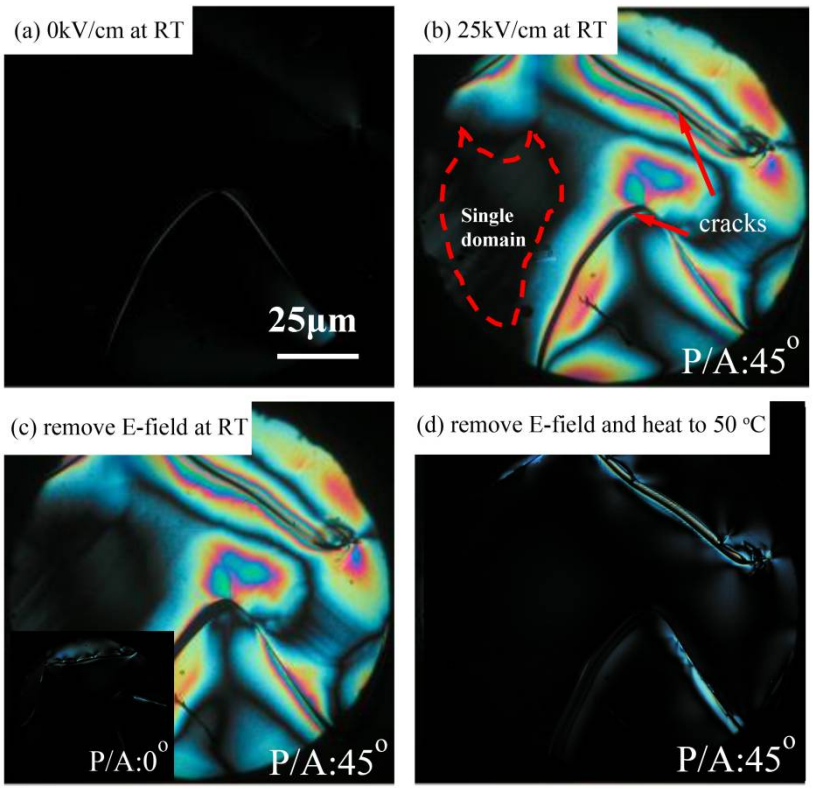

Figure 3. <001> oriented domain evolution of NBT-6BT-KNN crystal at the following different conditions in sequence (a–d): (**a**) initial state, electric field E = 0 kV/cm, at room temperature (RT); (**b**) positive increase of E to 25 kV/cm at RT; (**c**) remove electric field at RT; (**d**) heating to 50 °C after removing electric field.

Macroscopic Raman spectra contains local information via local phonon signals. Previous studies of NBT-based systems reveal that the changes in these Raman modes can reflect the crystal phase transition sensitively. Figure 5a,b shows the room temperature Raman spectra of unpoled (E = 0 kV/cm) and poled (E = 25 kV/cm) NBT-6BT-KNN crystals, respectively. The Raman spectra have been deconvoluted into six vibrational modes and the assignment of these modes is marked. The bands around 300 cm^{-1} are assigned to the Ti-O lattice vibration. The bands (around 527 cm^{-1} and 610 cm^{-1}) between 400 and 700 cm^{-1} are assigned to the TiO_6 octahedron vibration closely related to crystal symmetry [24,25]. After applying an electric field, two changes are clearly noticed. The relative intensity of 527 cm^{-1} and 610 cm^{-1} related to TiO_6 octahedron vibration changes significantly, and the vibration around the 610 cm^{-1} band is significantly weakened compared to the mode around 527 cm^{-1}. The behavior in these high frequency modes suggests a reduced degree of disorder [26], which further supports the electric-field-induced phase transition from pseudocubic a state to a ferroelectric tetragonal state. The electric-field-induced TiO_6 octahedron dynamics, in turn, affect the Ti-O band. The poled

crystal exhibits relatively more symmetry around the 300 cm^{-1} band, as compared to that of the unpoled crystal, which is also consistent with the reduced degree of disorder. When the poled crystals are heated to a temperature above T_d (T = 50 °C), the Raman spectra are then measured and shown in Figure 5c. It is clear that the Raman scattering profile almost completely evolves back to the initial state without poling, indicating that the temperature induced phase transitions from the polar tetragonal state back to the initial nonpolar pseudocubic state. These results are exactly consistent with the domain evolutions in Figure 3.

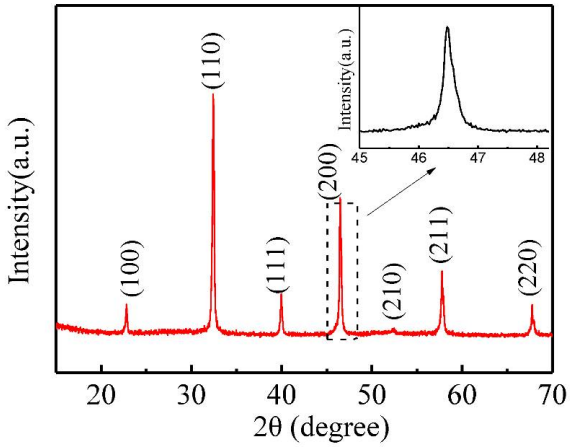

Figure 4. The XRD pattern of unpoled NBT-6BT-KNN crystal powder.

The sharply degenerated k_t and k_{31} at T_d for poled NBT-6BT-KNN crystals can now be well understood by the electric filed/temperature induced phase transition between the non-polar and polar states. When the crystals are poled at 25 kV /cm, the phase transitions occur from the pseudocubic non-polar phase to the tetragonal polar phase. However, when the crystals are heated to a temperature reaching above T_d, the ferroelectric polar phases are unstable and transform back to a pseudocubic non-polar phase, accompanied by a sharp degenerated k_t and k_{31} and a discontinuous variation in dielectric/loss curves at exactly T_d.

The piezoelectric and electromechanical coupling coefficients are strongly dependent on microstructural changes of nanodomains [27,28]. Piezoelectric force microscopy (PFM) is a very good experimental approach to detect ferroelectric nanoscale domains. In order to trace the origin of the ultrahigh electromechanical coupling coefficients k_t and k_{31} in NBT-6BT-KNN crystals, we used PFM to test the microscopic domain structure of NBT-6BT and NBT-6BT-KNN crystals. Figure 6 shows the PFM images of NBT-6BT-KNN and NBT-6BT crystals along the <001> direction. It can be seen that nano-regions of NBT-6BT-KNN exhibit a more dense and uniform distribution than that of NBT-6BT. In particular, the polar-regions became notably narrower with sizes, on average, of ~50 nm. As reflected in the amplify images (Figure 6c–d), the boundaries between regions became much smoother. These results clearly show that the addition of KNN to NBT-BT refines the size of the polar nanoregions and enhances their self-organization. Since the domain size is proportional to the square root of the domain wall energy, the smaller domain size makes it easily reoriented under external excitations, e.g., applied electric field or mechanical force [29,30]. Thus, the piezoelectric properties significantly improve with a decreasing domain size. It should be noted that these results have been found in $BaTiO_3$ ferroelectric single crystal [31–34]. Therefore, such refinement of ferroelectric domains in NBT-6BT-KNN crystal would lead to an increased domain-wall density and contribute to its ultrahigh value of electromechanical coupling performance.

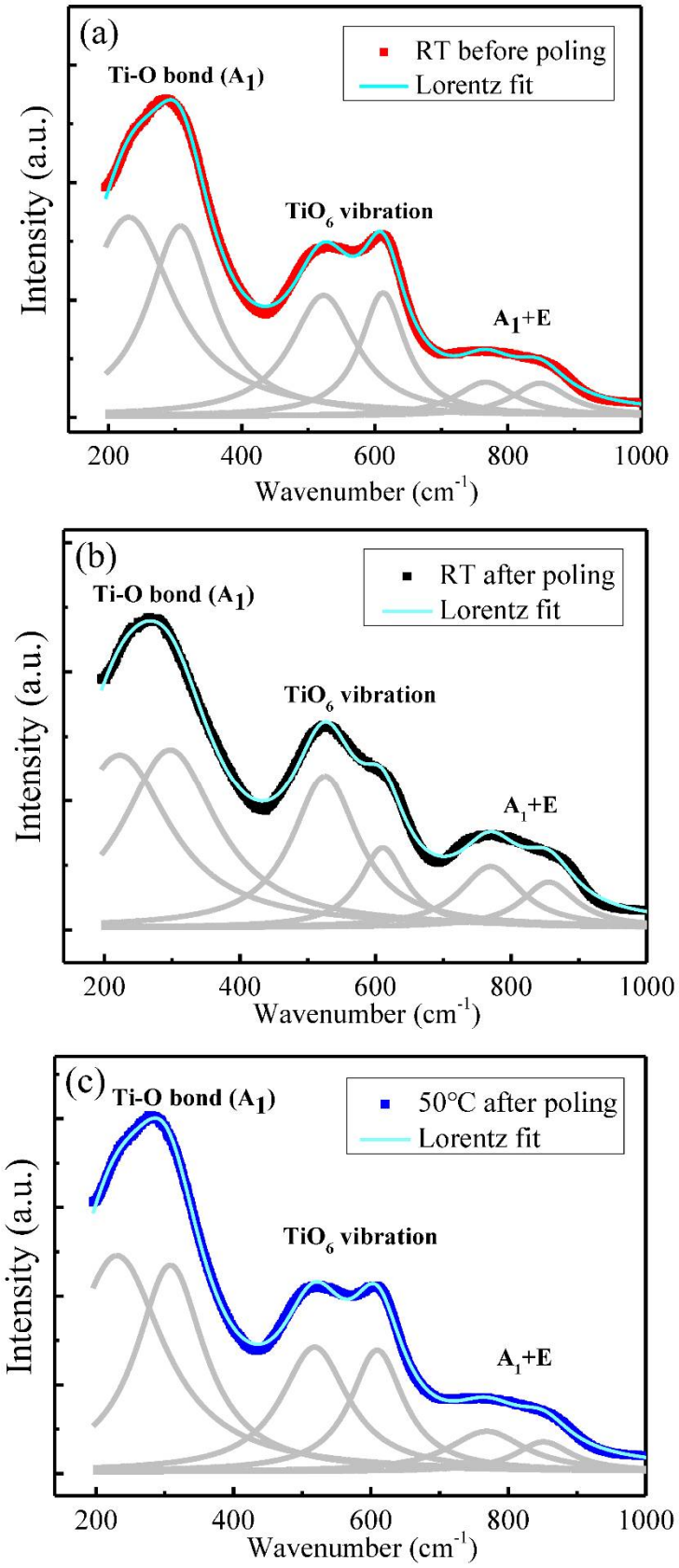

Figure 5. Raman spectra for <001>-oriented NBT-6BT-KNN crystal at different conditions: (**a**) room temperature (RT) before poling, (**b**) RT after poling, (**c**) 50 °C after poling.

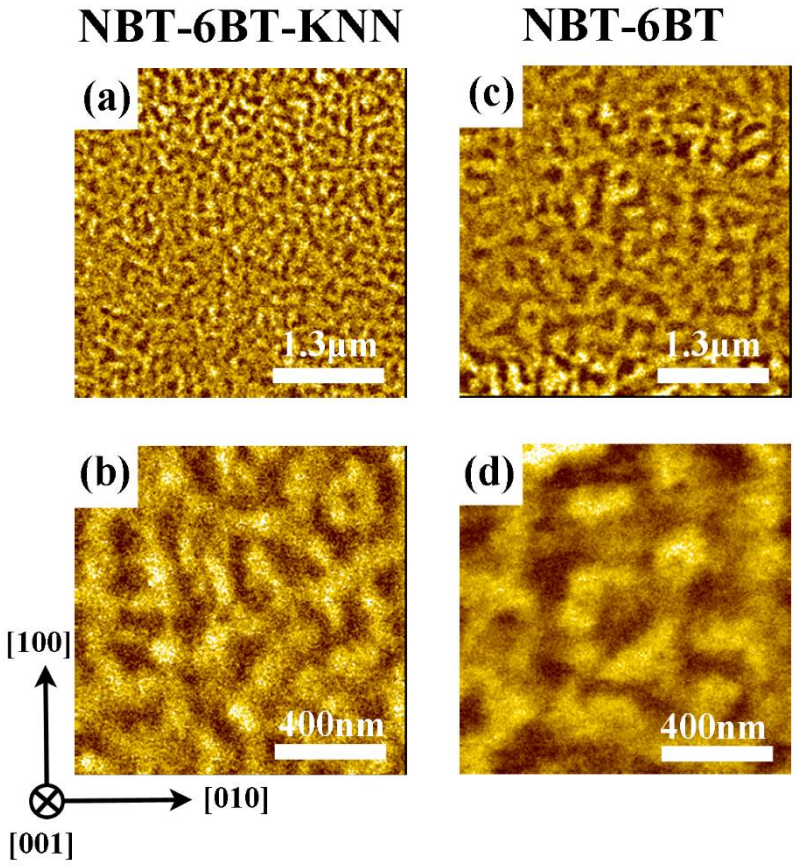

Figure 6. Piezoelectric force microscope (PFM) images of (**a**,**b**) NBT-6BT and (**c**,**d**) NBT-6BT-KNN crystals.

4. Conclusions

$0.93(Na_{1/2}Bi_{1/2})TiO_3$-$0.06BaTiO_3$-$0.01K_{1/2}Na_{1/2}NbO_3$ (NBT-6BT-KNN) single crystals show ultrahigh electromechanical coupling coefficients k_t and k_{31} reaching 69.0% and 45.7% respectively, which are superior to the PZT-5H lead-based ceramics of k_t ~ 60% and k_{31} ~ 39%. k_t and k_{31} vary little and exhibit a good temperature stability within this temperature range from −150 to 40 °C. When the temperature reaches above 45 °C, the value of k_t and k_{31} degenerates sharply to zero, which suggests a temperature induced tetragonal polar to pseudocubic non-polar phase transition verified by dielectric, polarizing microscope and Raman scattering measurements. The refinement of the ferroelectric domains and high domain-wall density was observed in the PFM results, which contributes to the ultrahigh electromechanical coupling of NBT-6BT-KNN crystals.

Author Contributions: For research articles with several authors, a short paragraph specifying their individual contributions must be provided. C.C. gave the onceptualization and wrote original draft preparation; L.Y. did data curation; X.J. (Xingan Jiang), X.H., X.G., N.T., K.S. joined formal analysis; X.J. (Xiangping Jiang), S.Z., H.L. supervised this work. All authors have read and agreed to the published version of the manuscript.

Funding: This work is financially supported by the National Natural Science Foundation of China (51862016, 51762024, 51602135), the Foundation of Jiangxi Provincial Education Department (GJJ190712). The author (Chao Chen) wishes to acknowledge the support from the Jiangxi Voyage Project and China Scholarship Council. The author also thanks Kunyu Zhao for performing the PFM measurements.

Conflicts of Interest: The authors declare no conflict of interest.

References

1. Hsu, H.S.; Benjauthrit, V.; Zheng, F.; Chen, R.; Huang, Y.; Zhou, Q.; Shung, K.K. PMN-PT–PZT composite films for high frequency ultrasonic transducer applications. *Sensor Actuat. A Phys.* **2012**, *179*, 121–124. [CrossRef]
2. Near, C.; Gentilman, R.; Pazol, B.; Fiore, D.; Serwatka, W.; Guyen, H.P.; Markowski, K.; Mcguire, P.; Bowen, L. Application of piezoelectric composites and net: Hape PZT ceramics as acoustic sensors and actuators. *J. Acoust. Soc. Am.* **1998**, *101*, 221–229. [CrossRef]
3. Rathod, V.T. A Review of Electric Impedance Matching Techniques for Piezoelectric Sensors, Actuators and Transducers. *Electronics* **2019**, *8*, 169.
4. Roedel, J. ChemInform Abstract: Giant Electric-Field-Induced Strains in Lead-Free Ceramics for Actuator Applications-Status and Perspective. *J. Electroceram.* **2012**, *29*, 71–93.
5. Rodel, J.; Jo, W.; Seifert, K.T.P.; Anton, E.M.; Damjanovic, D. Perspective on the Development of Lead-Free Piezoceramics. *J. Am. Ceram. Soc.* **2009**, *92*, 1153–1177.
6. Saito, Y.; Takao, H.; Tani, T.; Nonoyama, T.; Takatori, K.; Homma, T.; Nagaya, T.; Nakamura, M. Lead-free piezoceramics. *Nature* **2004**, *432*, 84–87. [CrossRef]
7. Shuai, C.; Zhang, B.; Lei, Z.; Wang, K. Enhanced insulating and piezoelectric properties of $0.7BiFeO_3$–$0.3BaTiO_3$ lead-free ceramics by optimizing calcination temperature: Analysis of Bi^{3+} volatilization and phase structures. *J. Mater. Chem. C.* **2018**, *6*, 3982–3989.
8. Wang, X.; Wu, J.; Xiao, D.; Zhu, J.; Cheng, X.; Zheng, T.; Zhang, B.; Lou, X.; Wang, X. Giant Piezoelectricity in Potassium-Sodium Niobate Lead-Free Ceramics. *J. Am. Chem. Soc.* **2014**, *136*, 2905–2910.
9. Kakimoto, K.I.; Akao, K.; Guo, Y.; Ohsato, H. Raman Scattering Study of Piezoelectric $(Na_{0.5}K_{0.5})NbO_3$-$LiNbO_3$ Ceramics. *Jpn. J. Appl. Phys.* **2005**, *44*, 7064–7067. [CrossRef]
10. Takenaka, T.; Maruyama, K.I.; Sakata, K. $(Bi_{1/2}Na_{1/2})TiO_3$-$BaTiO_3$ system for lead-free piezoelectric ceramics. *Jpn. J. Appl. Phys.* **1991**, *30*, 2236–2239. [CrossRef]
11. Cheng, M.; Guo, H.; Beckman, S.P.; Tan, X. Creation and Destruction of Morphotropic Phase Boundaries through Electrical Poling: A Case Study of Lead-Free $(Bi_{1/2}Na_{1/2})TiO_3$-$BaTiO_3$ Piezoelectrics. *Phys. Rev. Lett.* **2012**, *109*, 107601–107602.
12. Ahart, M.; Somayazulu, M.; Cohen, R.E.; Ganesh, P.; Dera, P.; Mao, H.K.; Hemley, R.J.; Ren, Y.; Liermann, P.; Wu, Z. Origin of morphotropic phase boundaries in ferroelectrics. *Nature* **2008**, *451*, 545–548. [CrossRef] [PubMed]
13. Daniels, J.E.; Jo, W.; Rödel, J.; Jones, J.L. Electric-field-induced phase transformation at a lead-free morphotropic phase boundary: Case study in a $93\%(Bi_{0.5}Na_{0.5})TiO_3$-$7\%BaTiO_3$ piezoelectric ceramic. *Appl. Phys. Lett.* **2014**. [CrossRef]
14. Ge, W.; Luo, C.; Zhang, Q.; Devreugd, C.P.; Ren, Y.; Li, J.; Luo, H.; Viehland, D. Ultrahigh electromechanical response in $(1-x)(Na_{0.5})Bi_{0.5})TiO_3$-$xBaTiO_3$ single-crystals via polarization extension. *J.Appl. Phys.* **2012**, *111*, 93501–93508. [CrossRef]
15. Wang, Y.; Luo, C.; Wang, S.; Chen, C.; Yuan, G.; Luo, H.; Viehland, D. Large Piezoelectricity in Ternary Lead-Free Single Crystals. *Adv. Electron. Mater.* **2020**, *6*, 1900949.
16. Peng, J.; Luo, H.; He, T.; Xu, H.; Lin, D. Elastic, dielectric, and piezoelectric characterization of $0.70Pb(Mg_{1/3}Nb_{2/3})O_3$–$0.30PbTiO_3$ single crystals. *Mater. Lett.* **2005**, *59*, 640–643. [CrossRef]
17. Yao, F.Z.; Wang, K.; Li, J.F. Comprehensive investigation of elastic and electrical properties of Li/Ta-modified (K,Na)NbO_3 lead-free piezoceramics. *J. Appl. Phys.* **2013**, *113*, 174101–174105. [CrossRef]
18. Huo, X.; Zheng, L.; Zhang, R.; Wang, R.; Wang, J. A high quality lead-free (Li, Ta) modified (K, Na)NbO_3 single crystal and its complete set of elastic, dielectric and piezoelectric coefficients with macroscopic 4mm symmetry. *Crystengcomm* **2014**. [CrossRef]
19. Huo, X.; Zhang, R.; Zheng, L.; Zhang, S.; Cao, W. (K, Na, Li)(Nb, Ta)O_3:Mn Lead-Free Single Crystal with High Piezoelectric Properties. *J. Am. Ceram Soc.* **2015**, *98*, 1829–1835. [CrossRef]
20. Zhou, D.; Lam, K.H.; Chen, Y.; Zhang, Q.; Chiu, Y.C.; Luo, H.; Dai, J.; Chan, H.L.W. Lead-free piezoelectric single crystal based 1-3 composites for ultrasonic transducer applications. *Sensor. Actuat. A Phys.* **2012**, *182*, 95–100.

21. Zheng, L.; Yi, X.; Zhang, S.; Jiang, W.; Yang, B.; Zhang, R.; Cao, W. Complete set of material constants of 0.95($Na_{0.5}Bi_{0.5}$)TiO_3-0.05$BaTiO_3$ lead-free piezoelectric single crystal and the delineation of extrinsic contributions. *Appl. Phys. Lett.* **2013**, *103*, 122905. [CrossRef]
22. Ma, C.; Tan, X.; Kleebe, H.J. In situ Transmission Electron Microscopy Study on the Phase Transitionsin Lead-Free (1−x)(Bi1/2Na1/2)TiO3–xBaTiO3 Ceramics. *J. Am. Ceram. Soc.* **2011**, *94*, 4040–4044. [CrossRef]
23. Chao, C.; Zhang, H.; Hao, D.; Huang, T.; Li, X.; Zhao, X.; Hu, Z.; Dong, W.; Luo, H. Electric field and temperature-induced phase transition in Mn-doped $Na_{1/2}Bi_{1/2}TiO_3$-5.O at.%$BaTiO_3$ single crystals investigated by micro-Raman scattering. *Appl. Phys. Lett.* **2014**, *104*, 142901–142902.
24. Glazer, A.M. The classification of tilted octahedra in perovskites. *Acta. Crystallographica* **1972**, *28*, 3384–3392. [CrossRef]
25. Kreisel, J.; Glazer, A.M.; Jones, G.; Thomas, P.A.; Abello, L.; Lucazeau, G. An x-ray diffraction and Raman spectroscopy investigation of A-site substituted perovskite compounds: The $(Na_{1-x}K_x)_{0.5}Bi_{0.5}TiO_3$ (0 <x <1) solid solution. *J. Phys. Condens. Matter* **2000**, *12*, 3267.
26. Maurya, D.; Pramanick, A.; Feygenson, M.; Neuefeind, J.C.; Priya, S. Effect of poling on nanodomains and nanoscale structure in A-site disordered lead-free piezoelectric $Na_{0.5}Bi_{0.5}TiO_3$-$BaTiO_3$. *J. Mater. Chem. C.* **2014**, *2*. [CrossRef]
27. Ge, W.; Hu, C.; Devreugd, C.; Li, J.; Viehl, D. Influence of $BaTiO_3$ Content on the Structure and Properties of $Na_{0.5}Bi_{i0.5}TiO_3$ Crystals. *J. Am. Ceram. Soc.* **2011**, *94*, 3084–3087. [CrossRef]
28. Yao, J.; Li, Y.; Ge, W.; Liang, L.; Li, J.; Viehland, D.; Zhang, Q.; Luo, H. Evolution of domain structures in $Na_{1/2}Bi_{1/2}TiO_3$ single crystals with $BaTiO_3$. *Phys. Rev. B.* **2011**, *83*, 54101–54107. [CrossRef]
29. Rossetti, G.A.; Khachaturyan, A.G.; Akcay, G.; Ni, Y. Ferroelectric solid solutions with morphotropic boundaries: Vanishing polarization anisotropy, adaptive, polar glass, and two-phase states. *J. Appl. Phys.* **2008**, *103*, 114113. [CrossRef]
30. Schoenau, K.A.; Schmitt, L.A.; Fuess, H.; Knapp, M.; Hoffmann, M.J. Nanodomain Structure of Pb($Zr_{1-x}Ti_x$)O_3 at Its Morphotropic Phase Boundary: Investigations From Local to Average Structure. *Phys. Rev. B* **2007**, *75*, 184117. [CrossRef]
31. Bai, F.; Li, J.; Viehland, D. Domain hierarchy in annealed (001)-oriented Pb($Mg_{1/3}Nb_{2/3}$)O_3-x%$PbTiO_3$ single crystals. *Appl. Phys. Lett.* **2004**, *85*, 2313–2315. [CrossRef]
32. Wada, S.; Kakemoto, H.; Tsurumi, T. Enhanced Piezoelectric Properties of Piezoelectric Single Crystals by Domain Engineering. *Mater. Trans.* **2004**, *45*, 178–187. [CrossRef]
33. Wada, S.; Tsurumi, T. Enhanced piezoelectricity of barium titanate single crystals with engineered domain configuration. *Brit. Ceram. Trans.* **2004**, *103*, 93–96.
34. Yako, K.; Kakemoto, H.; Tsurumi, T.; Wada, S. Enhanced Piezoelectric Properties of Barium Titanate Single Crystals by Domain Engineering. *Key Eng. Mater.* **2006**, *301*, 23–26.